Received 4 August 2020; accepted 16 September 2020. Date of publication 18 September 2020; date of current version 8 October 2020.
The review of this article was arranged by Editor M. J. Kumar.

Digital Object Identifier 10.1109/JEDS.2020.3024775

Analytical Study on the Breakdown Characteristics of Si-Substrated AlGaN/GaN HEMTs With Field Plates

JIANHUA LIU [1,2] (Graduate Student Member, IEEE), YU-FENG GUO [1,2] (Member, IEEE), JUN ZHANG [1,2] (Member, IEEE), JIAFEI YAO [1,2] (Member, IEEE), MAOLIN ZHANG [1,2] (Graduate Student Member, IEEE), CHENYANG HUANG[1,2], AND LING DU [1,2]

1 College of Electronic and Optical Engineering and College of Microelectronics, Nanjing University of Posts and Telecommunications, Nanjing 210023, China
2 National and Local Joint Engineering Laboratory of RF Integration and Micro-Assembly Technology, Nanjing University of Posts and Telecommunications, Nanjing 210023, China

CORRESPONDING AUTHOR: Y. GUO (e-mail: yfguo@njupt.edu.cn)

This work was supported in part by the National Natural Science Foundation of China under Grant 61874059, Grant 61904083, and Grant 61704084; in part by the China Post-Doctoral Science Foundation under Grant 2018M642291; in part by the Natural Science Foundation of Jiangsu Province under Grant BK20190237; in part by Opening Project of State Key Laboratory of Electronic Thin Films and Integrated Devices under Grant KFJJ201907; and in part by Postgraduate Research and Practice Innovation Program of Jiangsu Province under Grant KYCX19_0969.

ABSTRACT The breakdown voltage model of Si-substrated AlGaN/GaN HEMTs with gate and drain field plates is proposed in this work. The silicon substrate and GaN buffer are considered as the depletion region in the modeling process. The analytical model shows great simplicity and veracity. It gives physical insights into the breakdown characteristics of the AlGaN/GaN HEMTs. The avalanche breakdown occurs at the field plate's edge in lateral structure or at the interface in vertical structure. According to the analytical model, the relationship between the lateral breakdown and the vertical breakdown is demonstrated in this work. The breakdown location is affected by the variation of the structure parameters, including gate-to-drain distance, buffer thickness and field plates' lengths. With the aid of the analytical model, effective guidance for device optimization to achieve high performance can be obtained.

INDEX TERMS AlGaN/GaN HEMTs, gate and drain field plates, analytical model, breakdown voltage.

I. INTRODUCTION

Wide-Bandgap material GaN is gaining increasing attention for its attractive performance in high frequency and high power applications arising from its material properties [1]–[4]. Owing to the inherent polarization effect, two-dimension electron gas (2DEG) is induced at the AlGaN/GaN heterojunction interface. With high electron density and high electron mobility, the 2DEG gives rise to the extraordinary performance of AlGaN/GaN high electron mobility transistors (HEMTs) [5], [6].

Until now, many published works have investigated material quality, structure simulation, choice of substrate and processing techniques. Fewer efforts have been put on the analytical model of breakdown voltage, leaving room for further exploration. At present, most of the numerical simulations of AlGaN/GaN HEMTs are based on the TCAD tool, Synopsys Sentaurus. This consumes plenty of time and computing resources. Meanwhile, the fabrications and experiments of AlGaN/GaN HEMTs are costly and time consuming. Hence, exploration in the analytical model is essential, because it can provide physical insights in AlGaN/GaN HEMTs with simple approaches and reliable results. In 2005, Karmalkar proposed an analytical approach for GaN-based heterostructure field-effect transistors (HFETs) for the first time [7]. In 2006 they further explored the dependence of the electric field (E-Field) on applied drain voltage [8]. These models can offer guidance for device optimization. However, they are based on the curve

fitting of numerical simulations rather than the analytical solution of Poisson equations. By this approach, modeling complex device structures are challengeable and simulation results need to be obtained before modeling. After that, by solving Poisson equations, Mao *et al.* and Chen *et al.* proposed analytical models for AlGaN/GaN HEMTs operating in partial depletion mode [9], [10]. The potential and E-Field distributions can be obtained with a combination of two hypotheses introduced as boundary conditions at the passivation layer surface. Yang *et al.* proposed an analytical model for AlGaN/GaN HEMTs with partial silicon doping. Well fitted analytical results and simulation results can be obtained via this model [11]. As AlGaN/GaN HEMTs' wide application in high power region, its capacity to undertake high blocking voltage in off-state is a crucial parameter, evaluated as the breakdown voltage (BV). These models can obtain the potential and E-Field distributions at the heterojunction interface. However, there exist some challenges for them to predict BV due to the limitations of the models they proposed. To obtain the BV model, Mourad demonstrated an analytical approach for AlGaN/GaN HEMTs, by assuming that the potential distribution at the passivation surface as a proportional function with gate-to-drain distance [12]. In the modeling process, the passivation layer and barrier layer are considered. However, the channel layer, the buffer layer and the substrate are not involved. Demonstrated in the model is the breakdown at the heterojunction interface. The vertical breakdown is not considered, which is important in devices' breakdown characteristics, thus leaving room for further exploration. So far, no analytical model with consideration of buffer and substrate layers as depletion region has been proposed to investigate the E-Filed distribution and breakdown characteristics of AlGaN/GaN HEMTs with gate and drain field plates (GD-FPs), which deserves further exploration.

A two-dimension (2D) analytical model of AlGaN/GaN HEMTs on Si-substrate with GD-FPs based on the equivalent potential method (EPM) [13] is proposed in this work. The model is fully analytical without introducing simulation results as boundary conditions. Considering the GaN buffer layer and the silicon substrate in the modeling process, we can obtain a more complete analytical model. The potential and E-Field distributions for devices with various structure parameters can be obtained from the analytical model. Moreover, the BV model for Si-substrated AlGaN/GaN HEMTs with GD-FPs is proposed in this work, which gives physical insights into BV's variation with different device structures.

II. DEVICE STRUCTURE AND ANALYTICAL MODEL

The schematic cross-section of the AlGaN/GaN HEMTs with GD-FPs is shown in Fig. 1. The region of the AlGaN barrier layer under the gate electrode is recessed so that the AlGaN/GaN HEMTs can operate in enhancement-mode (E-mode). Metal-Insulator-Semiconductor (MIS) is widely used in AlGaN/GaN HEMTs gate structure engineering for

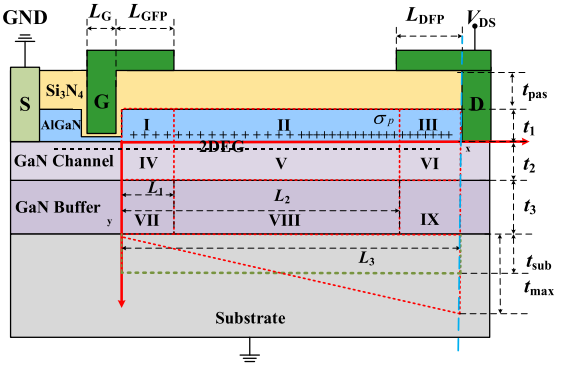

FIGURE 1. The schematic cross-section of the AlGaN/GaN HEMTs with GD-FPs.

its capacity to achieve low gate leakage current. Besides, Si_3N_4 material is employed as the gate dielectric and passivation layer [14], [15]. It is generally known that the E-Field peak at the gate or drain edge is the significant cause of the device's avalanche breakdown. So the FP structure is employed both at the gate and drain electrodes [16], [17]. The original E-Field peaks at the gate and drain edge are mitigated and new E-Field peaks come into being at the edge of gate FP (G-FP) and drain FP (D-FP), leading to more uniform potential and E-Field distributions. Although the D-FP has not been widely used in commercial AlGaN/GaN HEMTs, the D-FP structure leads to better performance in power applications [16]–[18], thus deserving further exploration.

When the device is biased in off-state ($V_S = 0V$, $V_{GS} = 0V$, $V_{DS} > 0V$), the barrier layer, the channel layer, the buffer layer and part of the substrate are depleted. The buffer layer can be seen as a p-type layer owing to the existence of the acceptor-type traps [19]–[21]. The potential distribution in the depletion region can be derived from 2D Poisson equations. To obtain the potential distribution, the depletion region can be divided into nine regions. Here, x measures the lateral distance relative to the right edge of the gate electrode and y measures the vertical distance relative to the AlGaN/GaN heterojunction interface. Besides, the point of the heterojunction interface at the gate right edge is set as zero. The depletion region consists of four layers, including the AlGaN barrier layer, GaN channel layer, Semi-Insulating GaN buffer layer and part of the silicon substrate. Owing to the existence of the GD-FPs, each layer can be divided into three regions in the lateral direction mathematically. The boundaries of them are denoted as L_0, L_1, L_2 and L_3 respectively. Where $L_0 = 0$ and $L_3 = L_{GD}$. The thickness of the Si_3N_4 passivation layer is denoted as t_{pas}. The thickness of the AlGaN barrier layer, GaN channel layer and Semi-Insulating GaN buffer layer are denoted as t_1, t_2 and t_3 respectively. As shown in Fig. 1, the depletion region in the substrate could be seen as a triangle, and the max thickness of the region is denoted as t_{max}. To simplify the modeling approach, the substrate depletion region is equivalent to a rectangle region. The equivalent thickness of the

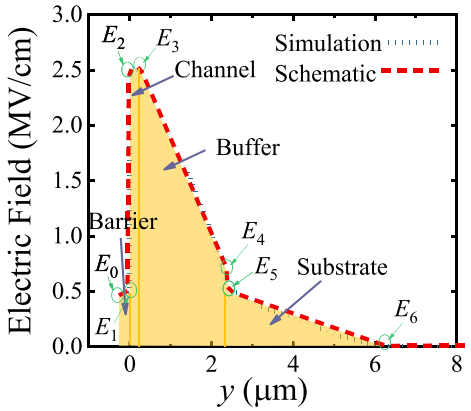

FIGURE 2. **The vertical E-Field along the cutline (blue dash line shown in Fig. 1).**

substrate depletion region is denoted as t_{sub}, which could be derived from $t_{\rm sub} = t_{\rm max}/2$. The vertical E-Field along the cutline is shown in Fig. 2. The potential difference along the cutline is the integral of the E-Field in the vertical direction. Hence, the area of the yellow region under the red dash line equals to the applied voltage. Meanwhile, the E-Field at the boundary of the substrate depletion region equals to zero. Thus, $t_{\rm sub}$ could be derived from the conditions above, yielding as Eq. (1). This is a common method used in analytical mode [22]. The $t_{\rm eff}$ and $t_{\rm eff0}$ are shown in the APPENDIX.

$$t_{sub} = \left(\left(t_{eff}^2 + t_{eff0}^2\right)^{0.5} - t_{eff}\right)/2 \tag{1}$$

N_1 and ε_1 are the intrinsic background carrier concentration and dielectric constant of the AlGaN barrier layer; ε_2 is the dielectric constant of GaN channel layer and GaN buffer layer; N_2 is the intrinsic background carrier concentration of GaN channel layer; P is the equivalent concentration of GaN buffer layer. The positive charge density in the GaN buffer layer is assumed to be invariable in the modeling process in this work, denoted as $Q(2 \times 10^{13}{\rm cm}^{-2})$. So P is a parameter relevant to the GaN buffer thickness, which can be expressed as $P = Q/t_3$. $P_{\rm sub}$ and $\varepsilon_{\rm sub}$ are the doping concentration and dielectric constant of the silicon substrate. The polarization charge density $\sigma_{\rm p}$ can be derived from the Al composition x and the thickness of the AlGaN barrier layer, based on polarization effect theory given by $\sigma_{\rm p} = |{\rm P_{PE}(Al_xGa_{1-x}N) + P_{SP}(Al_xGa_{(1-x)}N) - P_{SP}}$ (GaN) [6], [9]–[11]. The physical models used in the simulation include basic Poisson, drift-diffusion and current-continuity equations. The physical parameter models contain Shockley-Read-Hall for recombination, impact ionization for generation, high field-dependent mobility models, polarization model and carrier statistic model. The 2D potential function are denoted as $\varphi_{\rm i,j}(x, y)(L_{\rm j-1} < x < L_{\rm j}, d_{\rm i-1} < y < d_{\rm i}, {\rm i} = 1, 2, 3, {\rm j} = 1, 2, 3)$ in Region I to Region IX. And $l_1 = L_1, l_2 = L_2 - L_1, l_3 = L_3 - L_2, d_0 = -t_1, d_1 = 0, d_2 = t_2, d_3 = t_2 + t_3$. Considering the fact that the current in the device is neglectable before the breakdown, the charges considered in the depletion region are the ionized fixed charges in each layer [12], [23], [24]. The 2D potential functions could be obtained by solving the Poisson equations:

$$\frac{\partial^2\varphi_{1,j}(x,y)}{\partial x^2} + \frac{\partial^2\varphi_{1,j}(x,y)}{\partial y^2} = \frac{qN_1}{\varepsilon_1},\ {\rm j} = 1, 2, 3 \tag{2}$$

$$\frac{\partial^2\varphi_{2,j}(x,y)}{\partial x^2} + \frac{\partial^2\varphi_{2,j}(x,y)}{\partial y^2} = \frac{qN_2}{\varepsilon_2},\ {\rm j} = 1, 2, 3 \tag{3}$$

$$\frac{\partial^2\varphi_{3,j}(x,y)}{\partial x^2} + \frac{\partial^2\varphi_{3,j}(x,y)}{\partial y^2} = -\frac{qP}{\varepsilon_2},\ {\rm j} = 1, 2, 3 \tag{4}$$

To simplify the modeling process, the charge in the depletion region can be divided into two parts. The depletion region above the AlGaN/GaN interface is denoted as the top region. The depletion region below the AlGaN/GaN interface is denoted as the bottom region. By applying EPM, charges in the depletion region can be equivalent to the potentials at the passivation surface and the substrate as boundary conditions. Then the depletion region can be seen as neutral mathematically [13]. The modeling process is greatly simplified via the method. Hereby, the charges in the top region and the bottom region are equivalent to the potentials at passivation surface and substrate, denoted as $V_{\rm top}$ and $V_{\rm sub}$ respectively.

$$V_{top} = q\sigma_p\left(\frac{t_1}{\varepsilon_1} + \frac{t_{pas}}{\varepsilon_{pas}}\right) + qN_1\left(\frac{t_1^2}{2\varepsilon_1} + \frac{t_1 t_{pas}}{\varepsilon_{pas}}\right) \tag{5}$$

$$V_{sub} = qN_2\left(\frac{t_2^2}{2\varepsilon_2} + \frac{t_2 t_3}{\varepsilon_2} + \frac{t_2 t_{sub}}{\varepsilon_{sub}}\right) - qP\left(\frac{t_3^2}{2\varepsilon_1} + \frac{t_3 t_{sub}}{\varepsilon_{sub}}\right) - qP_{sub}\left(\frac{t_{sub}^2}{2\varepsilon_{sub}}\right) \tag{6}$$

According to EPM, the depletion region can be equivalent as neutral semiconductor mathematically. Thus, Laplace equations can be given out as Eq. (7).

$$\frac{\partial^2\varphi_{i,j}(x,y)}{\partial x^2} + \frac{\partial^2\varphi_{i,j}(x,y)}{\partial y^2} = 0,\ i = 1, 2, 3\ {\rm j} = 1, 2, 3 \tag{7}$$

The GaN channel layer and GaN buffer layer are the same semiconductor material. So, these two layers can be seen as an integral GaN layer for simplicity. The 2D potential function in the integral GaN layer is denoted as $\varphi_{4,{\rm j}}(x, y)(L_{\rm j-1} < x < L_{\rm j}, 0 < y < t_3, {\rm j} = 1, 2, 3)$ and can be expressed as Eq. (8).

$$\frac{\partial^2\varphi_{4,j}(x,y)}{\partial x^2} + \frac{\partial^2\varphi_{4,j}(x,y)}{\partial y^2} = 0,\ j = 1, 2, 3 \tag{8}$$

To solve the Laplace equations, boundary conditions need to be employed in the modeling process. According to electric flux continuity at AlGaN/Si_3N_4 passivation interface in the vertical direction, boundary condition yields as:

$$-\varepsilon_1\frac{\partial\varphi_{1,j}(x,y)}{\partial {\rm y}}\Big|_{y=d_0} = \begin{cases} \varepsilon_{pas}\dfrac{V_{\rm top}+\varphi_f(x)-\varphi_{1,j}(x,-t_1)}{t_{pas}}, & i = 1, 3 \\ \varepsilon_{pas}\dfrac{V_{\rm top}}{t_{pas}}, & i = 2 \end{cases} \tag{9}$$

Here, $\varphi_{\mathrm{f}}(x) = V_{\mathrm{G}},\ L_0 < x < L_1$; $\varphi_{\mathrm{f}}(x) = V_{\mathrm{DS}},\ L_2 < x < L_3$. When $L_1 < x < L_2$, the vertical E-Field can be evaluated as zero. The potential and the electric flux at the interface of AlGaN/GaN heterojunction are continuous in the vertical direction, leading to the formulas:

$$-\varepsilon_1 \frac{\partial \varphi_{1,j}(x,y)}{\partial \mathrm{y}}\Big|_{y=0} = -\varepsilon_2 \frac{\partial \varphi_{4,j}(x,y)}{\partial \mathrm{y}}\Big|_{y=0}.\ j = 1,2,3 \quad (10)$$

$$\varphi_{1,j}(x,0) = \varphi_{4,j}(x,0),\ j = 1,2,3 \quad (11)$$

Meanwhile, Eq. (12) can be obtained according to the concentration continuous at the heterojunction interface with EPM employed.

$$\frac{\partial^2 \varphi_{1,j}(x,y)}{\partial y^2}|_{y=0} = \frac{\partial^2 \varphi_{4,j}(x,y)}{\partial y^2}|_{y=0},\ j = 1,2,3 \quad (12)$$

According to the electric flux continuity at the interface of the GaN buffer layer and the silicon substrate, we can obtain Eq. (13).

$$-\varepsilon_2 \frac{\partial \varphi_{4,j}(x,y)}{\partial \mathrm{y}}|_{x=t_3} = \varepsilon_{\mathrm{sub}} \frac{\varphi_{4,j}(x,t_3) - V_{\mathrm{sub}}}{t_{sub}},\ j = 1,2,3 \quad (13)$$

The potential function $\varphi_{\mathrm{i,j}}(x,y)$ can be simplified as parabolic functions as shown in Eq. (14) based on Taylor's formula.

$$\varphi_{i,j}(x,y) = a_{i,j} + b_{i,j}x + c_{i,j}x^2,\ i = 1,4,\ j = 1,2,3 \quad (14)$$

So far, the vertical boundary conditions have been obtained via Eq. (9) to (13). By substituting them into Eq. (14), we can obtain the relationship between $a_{1,j}$ and $c_{1,j}$ yielding as:

$$2c_{1,j} = \frac{1}{T_j^2}\left(-a_{1,j} + V_j\right) \quad (15)$$

where T_j (j = 1, 2, 3) is the characteristic thickness of the device determined by device structure parameters, which can be expressed as Eq. (16). Since Region I and Region III are close to the edge of the gate and drain electrodes, a is a correction factor to take the edge effect into account [10]. Here, the parameters used in the modeling process are shown in the APPENDIX, including k_1, k_2, β_1, β_2, β_3, V_1, V_2 and V_3.

$$T_j = \begin{cases} \frac{\left(\left(t_1^2/2 + k_1 t_1 t_{pas}\right) + \beta_j\left(d_3^2/2 + k_2 d_3 t_{sub}\right)\right)}{1+\beta_j}, & j = 1,3 \\ \frac{\left(k_1 t_1 t_{pas} + \beta_2\left(d_3^2/2 + k_2 d_3 t_{sub}\right)\right)}{\beta_2}, & j = 2 \end{cases} \quad (16)$$

By substituting Eq. (15) and (16) into Eq. (7) at y=0, the partial differential function can be derived as Eq. (17).

$$\frac{\partial^2 \varphi_j(x,0)}{\partial x^2} - \frac{\varphi_j(x,0)}{T_j^2} = -\frac{V_j}{T_j^2},\ j = 1,2,3 \quad (17)$$

The 2D potential distribution at AlGaN/GaN heterojunction interface is derived as $\varphi_{\mathrm{j}}(x,0) = \varphi_{1,\mathrm{j}}(x,0) = \varphi_{4,\mathrm{j}}(x,0)$, j = 1, 2, 3. So, the potential distribution function at the heterojunction interface can be expressed as Eq. (18).

$$\varphi(x0) = \begin{cases} V_{11}\sinh\frac{x}{T_1} + V_{12}\sinh\frac{L_1-x}{T_1} + V_1, & L_0 \le x < L_1 \\ V_{21}\sinh\frac{x-L_1}{T_2} + V_{22}\sinh\frac{L_2-x}{T_2} + V_2, & L_1 \le x < L_2 \\ V_{31}\sinh\frac{x-L_2}{T_3} + V_{32}\sinh\frac{L_3-x}{T_3} + V_3, & L_2 \le x < L_3 \end{cases} \quad (18)$$

The gate electrode and the heterojunction interface is close enough that the potential drop across the gate dielectric is neglectable. Hence, the potential at the left boundary of Region I is V_{G}. Owing to the full depletion mode of AlGaN/GaN HEMTs, the potential at the right boundary of Region III can be evaluated as V_{DS}.

$$\varphi_1(0,0) = V_G,\ \varphi_3(L_2,0) = V_{DS} \quad (19)$$

The electric flux and potential at AlGaN/GaN heterojunction interface are continuous in the lateral direction, which yields:

$$\frac{\partial \varphi_j(x,0)}{\partial x}|_{x=L_j} = \frac{\partial \varphi_{j+1}(x,0)}{\partial x}\Big|_{x=L_j},\ j = 1,2 \quad (20)$$

$$\varphi_j(L_j,0) = \varphi_{j+1}(L_j,0),\ j = 1,2 \quad (21)$$

By substituting Eq. (18) into Eq. (19)-(21), the values of the parameters, V_{11}, V_{12}, V_{21}, V_{22}, V_{31} and V_{32} can be derived out, which are shown in the APPENDIX.

So far, based on EPM, the 2D potential distribution at the heterojunction interface is obtained in this section. The analytical approach is fully analytical without employing simulation results as boundary conditions. Therefore, it has the capacity to develop BV models for AlGaN/GaN HEMTs with GD-FPs.

III. E-FIELD AT THE HETEROJUNCTION INTERFACE

Based on the 2D potential distribution, we can obtain the E-Field distribution at the heterojunction interface, which has a significant impact on device's characteristics. For the AlGaN/GaN HEMTs with GD-FPs, the avalanche breakdown is triggered by the excessive E-Field peaks. To explore the breakdown mechanism of the devices, it is essential to analyze the E-Field distribution at the heterojunction interface. When the device operates in the full depletion mode, the E-Field distribution between the gate and drain electrodes can be derived from Eq. (18) by derivation, which yields:

$$E(x) = \begin{cases} \left(V_{11}\cosh\frac{x}{T_1} - V_{12}\cosh\frac{L_1-x}{T_1}\right)/T_1, & L_0 \le x < L_1 \\ \left(V_{21}\cosh\frac{x-L_1}{T_2} - V_{22}\cosh\frac{L_2-x}{T_2}\right)/T_2, & L_1 \le x < L_2 \\ \left(V_{31}\cosh\frac{x-L_2}{T_3} - V_{32}\cosh\frac{L_3-x}{T_3}\right)/T_3, & L_2 \le x < L_3 \end{cases} \quad (22)$$

Fig. 3 illustrates the potential and E-Field distributions at the heterojunction interface based on the analytical model and numerical simulation. As shown in Fig. 3, the analytical results are found out to be consistent with the simulation results obtained from Sentaurus. As illustrated in Fig. 3(a),

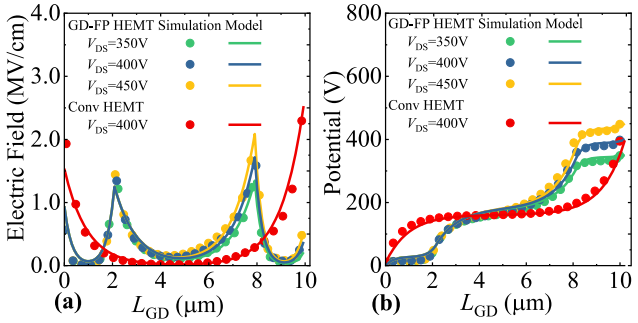

FIGURE 3. Analytical and numerical results of the E-Field distribution (a) and the potential distribution (b) at the heterojunction interface with various V_{DS} ($L_{GFP} = L_{DFP} = 2\mu m$, $L_{GD} = 10\mu m$, $t_2 = 0.3\mu m$, $t_{pas} = 100nm$, $N_1 = N_2 = 1 \times 10^{15} cm^{-3}$, $V_G = 0V$).

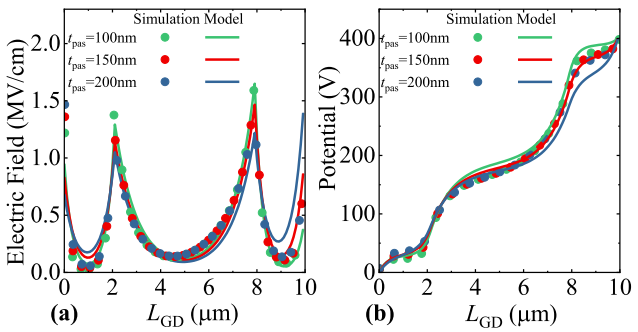

FIGURE 4. Analytical and numerical results of the E-Field distribution (a) and the potential distribution (b) at the heterojunction interface with various passivation layer thickness ($L_{GFP} = L_{DFP} = 2\mu m$, $L_{GD} = 10\mu m$, $t_2 = 0.3\mu m$, $V_G = 0V$, $V_{DS} = 400V$, $N_1 = N_2 = 1 \times 10^{15} cm^{-3}$).

E-Field peaks can be found at the gate electrode and the drain electrode of conventional AlGaN/GaN HEMTs which can be denoted as E_G and E_D respectively. With G-FP and D-FP been employed, the distribution of the E-Field is reshaped and two E-Field peaks form at the edges of the G-FP and D-FP denoted as E_{GFP} and E_{DFP} respectively. The original E-Field peaks, E_G and E_D, are mitigated. New E-Field peaks, E_{GFP} and E_{DFP}, generate at the E-Field valley leading to a more uniform E-Field distribution. With the increased V_{DS}, E_G, E_{GFP} and E_D increase slightly. However, E_{DFP} increases significantly. As the potential at the heterojunction interface is the integral of lateral E-Field, it is obvious that the increased voltage almost sustained by the region near the edge of D-FP. Hence, the edge of the D-FP is the most possible location where breakdown could occur in the lateral structure. As illustrated in Fig. 3(b), significant increments of the potential exist at the edge of the gate and drain electrodes of the conventional HEMTs. This is in accordance with the high E_G and E_D as shown in Fig. 3(a). Meanwhile, the potential is nearly invariable at the E-Field valley for conventional HEMTs, indicating that the region can hardly undertake the applied voltage. For AlGaN/GaN HEMTs with GD-FPs, the E-Field at the valley is enhanced leading to a more uniform potential distribution.

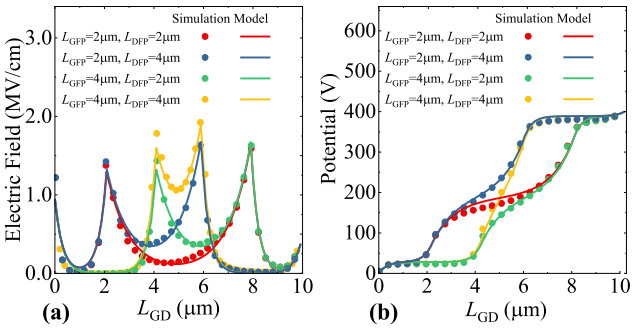

FIGURE 5. Analytical and numerical results of E-Field distribution (a) and the potential distribution (b) at the heterojunction interface with various FP lengths ($L_{GD} = 10\mu m$, $t_2 = 0.3\mu m$, $t_{pas} = 100nm$, $V_G = 0V$, $V_{DS} = 400V$, $N_1 = N_2 = 1 \times 10^{15} cm^{-3}$).

Fig. 4(a) illustrates the E-Field distribution of AlGaN/GaN HEMTs with different passivation layer thickness. With the decrease of the passivation layer thickness, E_G and E_D drop slightly, yet E_{GFP} and E_{DFP} increase significantly. This is for the reason that the spacing between the GD-FPs and heterojunction interface decreases with the thinner passivation layer. Hence, the FP has more significant modulation effects on the E-Field distribution. Fig. 4(b) shows the potential distribution of AlGaN/GaN HEMTs with different passivation layer thickness. The accuracy of the analytical results is well verified by the numerical simulations. Fig. 5 shows the E-Field and potential distributions of the HEMTs with various GD-FPs. The lengths of the G-FP and D-FP are chosen as the four sets, 2μm/2μm, 2μm/4μm, 4μm/2μm and 4μm/4μm respectively. As shown in Fig. 5(a), the locations of the E_{GFP} and E_{DFP} vary with different GD-FPs. The applied voltage is almost undertaken by the region between the G-FP and D-FP, which is also indicated in Fig. 5(b). The effective region to sustain the V_{DS} decreases with the extension of the GD-FPs. Therefore, the lengths of the GD-FPs need to be optimized for better performance.

IV. BREAKDOWN VOLTAGE

For power devices, the BV is limited by the most vulnerable points with high E-Field peaks. For the lateral structure of the AlGaN/GaN HEMTs with GD-FPs, there are two possible breakdown points at $x = L_1$ and $x = L_2$ respectively. In analytical models, the breakdown can be defined by the E-Field reaching the critical E-Field [12], [23], [24]. By substituting Eq. (22) into $E(x, 0) = E_C$, the lateral BV model can be obtained, which yields:

$$\begin{cases} BV_{GFP} = \frac{(E_{GaN}T_1 + V_{12})/\cosh(l_1/T_1) - \gamma}{\theta_1} \\ BV_{DFP} = \frac{E_{GaN}T_1 + \gamma_2 \cosh(l_3/T_1) - \gamma_3}{\theta_3 - \theta_2 \cosh(l_3/T_1)} \end{cases} \tag{23}$$

where θ_1, θ_2, θ_3, γ, γ_3 are shown in the APPENDIX. For the lateral breakdown, BV_{GFP} and BV_{DFP} indicate the breakdown occurs at the edge of G-FP and D-FP respectively. And the lateral breakdown voltage (BV_{lat}) is the minimum value between them.

$$BV_{lat} = \min\{BV_{GFP}, BV_{DFP}\} \tag{24}$$

For the vertical structure, the E_C of Silicon (E_{Si}) is one order lower than the E_C of GaN (E_{GaN}). Owing to the electric flux continuity at the GaN/Si interface, the breakdown could occur at the silicon side of the GaN/Si interface before the E-Field of the GaN buffer reaches E_{GaN}. Hence, the GaN/Si interface under the drain electrode is one possible breakdown location in the vertical structure. As shown in Fig. 2, the E-Field at the silicon side of the GaN/Si interface is denoted as E_5.The BV can be obtained as Eq. (25) by using $E_5 \leq E_{Si}$.

$$BV_{Si} = 2E_{Si}^2 \frac{\varepsilon_{sub}}{qP_{sub}} + 2E_{Si}\varepsilon_{sub}\left(\frac{t_1}{\varepsilon_1} + \frac{t_2+t_3}{\varepsilon_2}\right) + q\left(Pt_3\left(\frac{t_1}{\varepsilon_1} + \frac{2t_2+t_3}{2\varepsilon_2}\right) - \sigma_P\frac{t_1}{\varepsilon_1} - N_2t_2\left(\frac{t_1}{\varepsilon_1} + \frac{t_2}{2\varepsilon_2}\right)\right) \quad (25)$$

As illustrated in Fig. 2, the max E-Field peak exists at the AlGaN/GaN interface. This is another possible breakdown location in the vertical structure. By substituting $E_3 \leq E_{GaN}$, we can obtain the BV at the AlGaN/GaN interface yielding as Eq. (26).

$$BV_{GaN} = \frac{(\varepsilon_2 E_{GaN} - qPt_3)^2}{2qP_{sub}} + q\left(\frac{t_1(2(Pt_3\sigma_P - N_2t_2) - N_1t_1)}{2k_1} + \frac{Pt_3^2 - d_3(N_2t_2 - 2Pt_3)}{2k_2} - Pt_3t_{eff}\right) + \varepsilon_2 E_{GaN}t_{eff} \quad (26)$$

The vertical breakdown is determined by the minimum between BV_{Si} and BV_{GaN} yielding as Eq. (27).

$$BV_{ver} = \min\{BV_{GaN}, BV_{Si}\} \quad (27)$$

In this article, the E_{GaN} and E_{Si} are set around 3×10^6V/cm and 3×10^5V/cm respectively [25]–[28]. The BV of the AlGaN/GaN HEMTs with GD-FPs is limited by the minimum BV between BV_{lat} and BV_{ver}, which can be given by:

$$BV = min[BV_{lat}, BV_{ver}] \quad (28)$$

To verify the credibility and reliability of the analytical solution and numerical approach in this work, the results of the published experiments are shown in Fig. 6(a) and (b) [29], [30]. When l_1 and l_3 are set to zero, the analytical model of AlGaN/GaN HEMTs with GD-FPs can degenerate into the model of conventional HEMTs. As shown in Fig. 6(a), the analytical model and numerical simulations are in accordance with the experiments demonstrated in the published works. The analytical results of the relationship between on-resistance ($R_{on.sp}$) and L_{GD} are illustrated in Fig. 6 (b) based on the Eq. (29).

$$R_{on,sp} = \frac{(L_{SG} + L_G + L_{GD})^2}{q\mu_n\sigma_P} + R_{con} \quad (29)$$

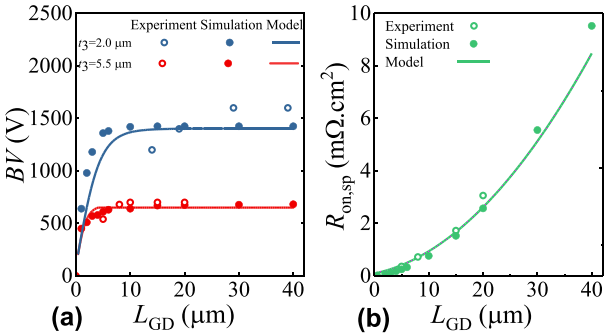

FIGURE 6. The *BV* (a) and $R_{on,sp}$ (b) of conventional AlGaN/GaN HEMTs with various gate-to-drain distance. (t_{pas} = 100nm, t_2 = 0.3μm, $N_1 = N_2 = 1 \times 10^{15}$cm^{-3}, V_G = 0V).

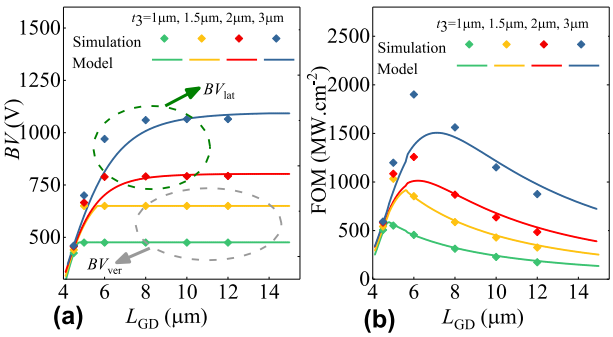

FIGURE 7. The *BV* (a) and FOM (b) of AlGaN/GaN HEMTs with GD-FPs with various gate-to-drain distance. ($L_{GFP} = L_{DFP}$ = 2μm, t_{pas} = 100nm, t_2 = 0.3μm, $N_1 = N_2 = 1 \times 10^{15}$cm^{-3}, V_G = 0V).

where L_{SG} and L_G are the lengths of the source-to-gate region and the length of the channel under the gate electrode respectively. R_{con} is the contact resistance of the source and drain electrodes. As shown in Fig. 6, analytical results and numerical simulations are in good agreement with the experiment results, which is a valid proof for the reliability of the analytical approach and numerical simulations.

As shown in Fig. 7(a), BV increases with the increment of L_{GD} and saturates with a specific gate-to-drain distance. The trend of the BV versus L_{GD} is in agreement with published works [29], [30]. When the buffer layer is thin, the breakdown tends to happen in the vertical structure. Hence, the BV is invariable with further increased L_{GD}. As illustrated in Fig. 7(a), AlGaN/GaN HEMTs with 1.0 μm and 1.5μm GaN buffer break down in vertical structure at 470V and 645V respectively. It indicates that the thicker GaN buffer layer can undertake higher BV. With further increased buffer thickness, the vertical breakdown is hard to happen and the breakdown tends to happen in the lateral structure. The BV increases linearly with the increment of L_{GD}, and also saturate at a specific value. This is for the reason that when the L_{GD} is long enough, the middle part of the gate to drain region can hardly undertake the applied voltage. As shown in Fig. 7(a), the BV of AlGaN/GaN HEMTs with 2.0 μm and 3.0 μm GaN buffer saturate at 800V and 1060V respectively. With the simple and accurate breakdown voltage model, the figure of merit (FOM) can be obtained

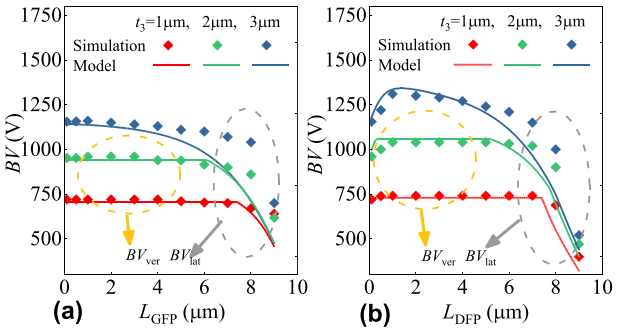

FIGURE 8. The *BV* of AlGaN/GaN HEMTs with various G-FP lengths (L_{DFP} = 0μm) (a) and D-FP lengths (L_{GFP} = 0μm) (b). (L_{GD} = 10μm, t_{pas} = 100nm, t_2 = 1μm, $N_1 = N_2 = 1 \times 10^{15}$cm^{-3}, V_G = 0V).

from FOM=$BV^2/R_{on,sp}$. Although slight imperfections can be found at the peaks of the FOM, the trend of the FOM versus L_{GD} shows good agreements between analytical results and numerical simulations. As is illustrated in Fig. 7(b), the FOM's peaks can be achieved at L_{GD} = 4.9μm, 5.8μm, 6.2μm and 7.1μm respectively with different buffer thicknesses. The corresponding L_{GD} to obtain the FOM peaks increase with the increment of buffer thickness. The values of the FOM peaks also increase with the thicker buffer layer. As mentioned before, the BV saturate with continuously increased L_{GD}. Yet the on-resistance would further increase with the increment of L_{GD}. Hence, the FOM of the devices decrease apparently after reaching the peak. Hence, to make full use of the wafer area and achieve higher BV, well-matched L_{GD} and buffer thickness should be cautiously chosen. The optimized L_{GD} and buffer thickness can be chosen where the FOM peaks occur.

As shown in Fig. 8, the BV of AlGaN/GaN HEMTs varies with different FP parameters. In Fig. 8(a), when the GaN buffer is thin, at 1-2μm, breakdown occurs in the vertical structure. Hence, the BV is invariable with increased L_{GFP}. When the GaN buffer is thick enough, BV would slightly drop with increased L_{GFP}. It is because that when the device is in full depletion mode, the breakdown can hardly happen at the edge of the G-FP. Meanwhile, the region under the G-FP barely undertakes the applied voltage. Hence, the increment of the L_{GFP} only decreases the distance to sustain the applied voltage. This is equivalent to that the L_{GD} decreases with L_{GFP} and L_{DFP} kept invariable. Moreover, when the L_{GFP} is long enough, nearly reaching L_{GD}, the BV drop significantly. As illustrated in Fig. 8(b), when the buffer is thick enough, at 3μm, the BV significantly increases with the increased L_{DFP}. This indicates that when the device is in full depletion mode, the edge of the D-FP is the most possible location to break down in the lateral structure. With D-FP introduced, the E_D is mitigated and the E-Field distribution becomes uniform, leading to higher BV. After that, the BV begins to drop significantly with further increased L_{DFP}. This is also due to that the distance to sustain the applied voltage decreases with overlarge L_{DFP}. When the buffer is thin enough, at 1-2μm as shown in Fig. 8(b), the BV is determined by the vertical breakdown. Hence, the BV barely increases with the increment of L_{DFP}. To achieve high BV, the length of D-FP should be optimized according to buffer thickness. As shown in Fig. 8(b), when the GaN buffer is 3μm, L_{DFP} should be chosen as 1.2μm.

V. CONCLUSION

By solving Laplace equations, we can obtain the analytical model of the potential and E-Field distributions of AlGaN/GaN HEMTs on Si-substrate with GD-FPs. The analytical results are in good agreement with numerical simulations. Moreover, the breakdown voltage model of AlGaN/GaN HEMTs with GD-FPs is proposed in this work, which shows good simplicity and accuracy. Considering the GaN buffer layer and the silicon substrate in the modeling approach, a more complete analytical model can be obtained in this work. The breakdown voltage model provides clear physical insights into the breakdown characteristics of AlGaN/GaN HEMTs, which is determined by the lateral breakdown and vertical breakdown simultaneously. When the GaN buffer is thin enough, the breakdown tends to happen in the vertical structure, and the BV is invariable with further increased gate-to-drain distance. Therefore, it is difficult to achieve high BV with a thin GaN buffer layer. With thicker GaN buffer, the vertical breakdown is hard to happen, and the BV is determined by the lateral breakdown. To achieve better performance, the well-matched gate-to-drain distance, buffer thickness and FPs' lengths can be obtained according to the analytical model. Therefore, accurate prediction and effective guidance can be offered by the breakdown voltage model, which are of great importance for devices' optimization.

APPENDIX

$$
\begin{aligned}
t_{eff} &= t_1/k_1 + (t_2 + t_3)/k_2 \\
t_{eff0}^2 &= (2V_{DS}/q + t_1(N_1 t_1 - 2(Pt_3\sigma_P - N_2 t_2))/k_1 \\
&\quad + d_3(N_2 t_2 - 2Pt_3)/k_2 + Pt_3^2/k_2\Big)/qP_{sub} \\
T &= T_2/T_1,\ k = \varepsilon_1/\varepsilon_2,\ k_1 = \varepsilon_1/\varepsilon_{pas},\ k_2 = \varepsilon_2/\varepsilon_{sub} \\
\beta_1 &= \beta_3 = \big(k_1 t_{\text{pas}} - d_1\big)a/(k(k_2 t_{sub} + d_3)), \\
\beta_2 &= k_1 t_{\text{pas}}/(k(k_2 t_{sub} + d_3)) \\
V_1 &= V_3 = \big(\varphi_f(x) + \varphi_{top} + \beta_1\varphi_{sub}\big)/(1 + \beta_1), \\
V_2 &= \big(\varphi_{top} + \beta_2\varphi_{sub}\big)/(1 + \beta_2) \\
V_{11} &= (\omega_1 + V_{31}T - (V_2 - V_3)Tcoth(l_3/T_1)/T_1)/\omega_2 \\
V_{12} &= (V_G - V_1)/sinh(l_1/T_1) \\
V_{21} &= V_{11}(Tcosh(l_1/T_1) + sinh(l_1/T_1)coth(l_2/T_2)) \\
&\quad + (V_1 - V_2)coth(l_2/T_2) - V_{12}T \\
V_{22} &= (V_{11}sinh(l_1/T_1) + (V_1 - V_2))/sinh(l_2/T_2) \\
V_{31} &= (V_{\text{DS}} - V_3)/sinh(l_3/T_1) \\
V_{32} &= (V_{21}sinh(l_2/T_2) + V_2 - V_3)/sinh(l_3/T_1) \\
\theta_1 &= T(\beta_1/sinh(l_3/T_1) + coth(l_3/T_1))/(\omega_2(1 + \beta_1)) \\
\theta_2 &= (\theta_1 sinh(l_2/T_2) - 1/((1 + \beta_1)))/sinh(l_3/T_1) \\
\theta_3 &= \Big(V_{DS} - \big(V_{top+}\beta_1 V_{sub} + V_{DS}\big)/(1 + \beta_1)\Big)/sinh(l_3/T_1) \\
\gamma &= \omega_3/\omega_2 \\
\gamma_1 &= \gamma(Tcosh(l_1/T_1) + sinh(l_1/T_1)coth(l_2/T_2))
\end{aligned}
$$

$$
\begin{aligned}
&+ (V_1 - V_2)coth(l_2/T_2) - V_{12}T \\
\gamma_2 &= \left(\gamma_1 sinh(l_2/T_2) + V_2 - \left(V_{top+}\beta_1 V_{sub}\right)/(1+\beta_1)\right)/ \\
&\quad sinh(l_3/T_1) \\
\gamma_3 &= \beta_1 sinh(l_3/T_1)V_{DS}/(1+\beta_1) \\
\omega_1 &= (cosh(l_2/T_2) + Tcoth(l_3/T)sinh(l_2/T_2))(V_1 - V_2) \\
&\quad \times V_{12}Tcoth(l_2/T_2) \\
&\quad + (V_1 - V_2)/sinh(l_2/T_2) \\
\omega_2 &= T^2 cosh(l_1/T_1)sinh(l_2/T_2)coth(l_3/T_1) \\
&\quad - sinh(l_1/T_1)/sinh(l_2/T_2) \\
&\quad + cosh(l_2/T_2) \\
&\quad \times (Tsinh(l_1/T_1)coth(l_3/T_1) + sinh(l_1/T_1)coth(l_2/T_2) \\
&\qquad + Tcosh(l_1/T_1)) \\
\omega_3 &= \omega_1 - \left(\left(V_{top} + \beta_1 V_{sub}\right)/sinh(l_3/T_1) + coth(l_3/T)\right. \\
&\qquad \left. \times \left(V_{top} + \beta_1 V_{sub}\right)\right)T/(1+\beta_1) \\
&\quad - V_2 Tcoth(l_3/T).
\end{aligned}
$$

REFERENCES

[1] S. H. Sohel *et al.*, "Polarization engineering of AlGaN/GaN HEMT with graded InGaN sub-channel for high-linearity X-band applications," *IEEE Electron Device Lett.*, vol. 40, no. 4, pp. 522–525, Apr. 2019, doi: 10.1109/LED.2019.2899100.

[2] D. Kim, H. Park, S. Eom, J. Jeong, H. Cha, and K. Seo, "Ka-band MMIC using AlGaN/GaN-on-Si with recessed high-*k* dual MIS structure," *IEEE Electron Device Lett.*, vol. 39, no. 7, pp. 995–998, Jul. 2018, doi: 10.1109/LED.2018.2834223.

[3] M. Alshahed *et al.*, "Low-dispersion, high-voltage, low-leakage GaN HEMTs on native GaN substrates," *IEEE Trans. Electron Devices*, vol. 65, no. 7, pp. 2939–2947, Jul. 2018, doi: 10.1109/TED.2018.2832250.

[4] A. Rawat, V. K. Surana, M. Meer, N. Bhardwaj, S. Ganguly, and D. Saha, "Gate current reduction and improved DC/RF characteristics in GaN-Based MOS-HEMTs using thermally grown TiO_2 as a dielectric," *IEEE Trans. Electron Devices*, vol. 66, no. 6, pp. 2557–2562, Jun. 2019, doi: 10.1109/TED.2019.2910608.

[5] W. E. Muhea, F. M. Yigletu, R. Cabré-Rodon, and B. Iñiguez, "Analytical model for schottky barrier height and threshold voltage of AlGaN/GaN HEMTs with piezoelectric effect," *IEEE Trans. Electron Devices*, vol. 65, no. 3, pp. 901–907, Mar. 2018, doi: 10.1109/TED.2018.2789822.

[6] J. P. Ibbetson, P. T. Fini, K. D. Ness, S. P. DenBaars, J. S. Speck, and U. K. Mishra, "Polarization effects, surface states and the source of electrons in AlGaN/GaN heterostructure field-effect transistors," *Appl. Phys. Lett.*, vol. 77, no. 2, pp. 250–252, Jul. 2000, doi: 10.1063/1.126940.

[7] S. Karmalkar, M. S. Shur, G. Simin, and M. A. Khan, "Field-plate engineering for HFETs," *IEEE Trans. Electron Devices*, vol. 52, no. 12, pp. 2534–2540, Dec. 2005, doi: 10.1109/TED.2005.859568.

[8] S. Karmalkar and N. Soudabi, "A closed-form model of the drain-voltage dependence of the off-state channel electric field in a HEMT with a field plate," *IEEE Trans. Electron Devices*, vol. 53, no. 10, pp. 2430–2437, Oct. 2006, doi: 10.1109/TED.2006.882273.

[9] W. Mao *et al.*, "A two-dimensional fully analytical model with polarization effect for off-state channel potential and electric field distributions of GaN-based field-plated high electron mobility transistor," *Chin. Phys. B*, vol. 23, no. 8, Jun. 2014, Art. no. 087305, doi: 10.1088/1674-1056/23/8/087305.

[10] T. Chen, Q. Zhou, D. Wei, C. Dong, W. Chen, and B. Zhang, "Physics-based 2-D analytical model for field-plate engineering of AlGaN/GaN power HFET," *IEEE Trans. Electron Devices*, vol. 66, no. 1, pp. 116–125, Jan. 2019, doi: 10.1109/TED.2018.2873810.

[11] L. Yang, B. Duan, Y. Wang, and Y. Yang, "Analytical models for the electric field and potential of AlGaN/GaN HEMT with partial silicon doping," *Superlattices Microstruct.*, vol. 128, pp. 349–357, Feb. 2019, doi: 10.1016/j.spmi.2019.02.010.

[12] K. Mourad, A. Telia, and A. Soltani, "Analytical modeling and analysis of $Al_mGa_{1-m}N$/GaN HEMTs employing both field-plate and high-*k* dielectric stack for high-voltage operation," *J. Comput. Electron.*, vol. 12, no. 3, pp. 501–510, Jun. 2013, doi: 10.1007/s10825-013-0468-5.

[13] J. Liu *et al.*, "Analytical model for the potential and electric field distributions of AlGaN/GaN HEMTs with gate-connected FP based on equivalent potential method," *Superlattices Microstruct.*, vol. 138, Nov. 2019, Art. no. 106327, doi: 10.1016/j.spmi.2019.106327.

[14] S. Huang *et al.*, "High uniformity normally-off GaN MIS-HEMTs fabricated on ultra-thin-barrier AlGaN/GaN hetero-structure," *IEEE Electron Device Lett.*, vol. 37, no. 12, pp. 1617–1620, Dec. 2016, doi: 10.1109/LED.2016.2617381.

[15] Y. Shi *et al.*, "Normally off GaN-on-Si MIS-HEMTs fabricated with LPCVD-SiN_x passivation and high-temperature gate recess," *IEEE Trans. Electron Devices*, vol. 63, no. 2, pp. 614–619, Feb. 2016, doi: 10.1109/TED.2015.2510630.

[16] S. Karmalkar, J. Deng, and M. S. Shur, "RESURF AlGaN/GaN HEMT for high voltage power switching," *IEEE Electron. Device Lett.*, vol. 22, no. 8, pp. 373–375, Aug. 2001, doi: 10.1109/55.936347.

[17] A. Soni and M. Shrivastava, "Novel drain-connected field plate GaN HEMT designs for improved V_{BD}–R_{ON} tradeoff and RF PA performance," *IEEE Trans. Electron Devices*, vol. 67, no. 4, pp. 1718–1725, Mar. 2020, doi: 10.1109/TED.2020.2976636.

[18] B. Liao, Q. Zhou, J. Qin, and H. Wang, "Simulation of AlGaN/GaN HEMTs' breakdown voltage enhancement using gate field-plate, source field-plate and drain field plate," *Electronics*, vol. 8, no. 4, pp. 1–11, Mar. 2019, doi: 10.3390/electronics8040406.

[19] V. Joshi, S. P. Tiwari, and M. Shrivastava, "Part I: Physical insight into carbon-doping-induced delayed avalanche action in GaN buffer in AlGaN/GaN HEMTs," *IEEE Trans. Electron Devices*, vol. 66, no. 1, pp. 561–569, Jan. 2019, doi: 10.1109/TED.2018.2878770.

[20] T. Kabemura, S. Ueda, Y. Kawada, and K. Horio, "Enhancement of breakdown voltage in AlGaN/GaN HEMTs: Field plate plus high-*k* passivation layer and high acceptor density in buffer layer," *IEEE Trans. Electron Devices*, vol. 65, no. 9, pp. 3848–3854, Jul. 2018, doi: 10.1109/TED.2018.2857774.

[21] N. K. Subramani, J. Couvidat, A. A. Hajjar, J. Nallatamby, and R. Quéré, "Low-frequency drain noise characterization and TCAD physical simulations of GaN HEMTs: Identification and analysis of physical location of traps," *IEEE Electron. Device Lett.*, vol. 39, no. 1, pp. 107–110, Jan. 2018, doi: 10.1109/LED.2017.2771407.

[22] M. Qiao *et al.*, "Analytical modeling for a novel triple RESURF LDMOS with N-top layer," *IEEE Trans. Electron Devices*, vol. 62, no. 9, pp. 2933–2939, Sep. 2015, doi: 10.1109/TED.2015.2448120.

[23] K. Yang *et al.*, "A novel variation of lateral doping technique in SOI LDMOS with circular layout," *IEEE Trans. Electron Devices*, vol. 65, no. 4, pp. 1447–1452, Apr. 2018, doi: 10.1109/TED.2018.2808193.

[24] Y. Wang, X. F. Meng, P. P. Tang, and S. F. Cui, "Analytical model and optimization for variable drift region width SOI LDMOS device," *IEEE Trans. Electron Devices*, vol. 63, no. 11, pp. 4352–4358, Sep. 2016, doi: 10.1109/TED.2016.2607423.

[25] A. Aminbeidokhti, A. A. Orouji, and M. Rahimian, "High-voltage and RF performance of SOI MESFET using controlled electric field distribution," *IEEE Trans. Electron Devices*, vol. 59, no. 10, pp. 2842–2845, Oct. 2012, doi: 10.1109/TED.2012.2208116.

[26] T. Maeda *et al.*, "Parallel-plane breakdown fields of 2.8–3.5 MV/cm in GaN-on-GaN p-n junction diodes with double-side-depleted shallow bevel termination," in *IEDM Tech. Dig.*, Dec. 2018, pp. 689–693, doi: 10.1109/IEDM.2018.8614669.

[27] B. J. Baliga, "Gallium nitride devices for power electronic applications," *Semicond. Sci. Technol.*, vol. 28, no. 7, pp. 1–8, Jun. 2013, doi: 10.1088/0268-1242/28/7/074011.

[28] L. Cao *et al.*, "Experimental characterization of impact ionization coefficients for electrons and holes in GaN grown on bulk GaN substrates." *Appl. Phys. Lett.*, vol. 112, no. 26, Jun. 2018, Art. no. 262103, doi: 10.1063/1.5031785.

[29] P. Srivastava *et al.*, "Record breakdown voltage (2200 V) of GaN DHFETs on Si with 2μm buffer thickness by local substrate removal," *IEEE Electron Device Lett.*, vol. 32, no. 1, pp. 30–32, Jan. 2011, doi: 10.1109/LED.2010.2089493.

[30] H. Nicolas *et al.*, "Above 2000 V breakdown voltage at 600 K GaN-on-silicon high electron mobility transistors," *Phys. Status Solidi*, vol. 213, no. 4, pp. 873–877, Apr. 2016, doi: 10.1002/pssa.201532572.